AIP | Applied Physics Letters

Analytical modeling and numerical simulation of the short-wave infrared electron-injection detectors

Yashar Movassaghi, Vala Fathipour, Morteza Fathipour, and Hooman Mohseni

Citation: Applied Physics Letters **108**, 121102 (2016); doi: 10.1063/1.4944602
View online: http://dx.doi.org/10.1063/1.4944602
View Table of Contents: http://scitation.aip.org/content/aip/journal/apl/108/12?ver=pdfcov
Published by the AIP Publishing

Analytical modeling and numerical simulation of the short-wave infrared electron-injection detectors

Yashar Movassaghi,[1,a)] Vala Fathipour,[2,a)] Morteza Fathipour,[1] and Hooman Mohseni[2]
[1]*Modeling and Simulation of Semiconductor Devices Laboratory, Department of Electrical and Computer Engineering of the University of Tehran, Tehran 1417466191, Iran*
[2]*Bio-Inspired Sensors and Optoelectronics Laboratory, Northwestern University, 2145 Sheridan Rd, Evanston, Illinois 60208, USA*

(Received 24 November 2015; accepted 9 March 2016; published online 21 March 2016)

This paper describes comprehensive analytical and simulation models for the design and optimization of the electron-injection based detectors. The electron-injection detectors evaluated here operate in the short-wave infrared range and utilize a type-II band alignment in InP/GaAsSb/InGaAs material system. The unique geometry of detectors along with an inherent negative-feedback mechanism in the device allows for achieving high internal avalanche-free amplifications without any excess noise. Physics-based closed-form analytical models are derived for the detector rise time and dark current. Our optical gain model takes into account the drop in the optical gain at high optical power levels. Furthermore, numerical simulation studies of the electrical characteristics of the device show good agreement with our analytical models as well experimental data. Performance comparison between devices with different injector sizes shows that enhancement in the gain and speed is anticipated by reducing the injector size. Sensitivity analysis for the key detector parameters shows the relative importance of each parameter. The results of this study may provide useful information and guidelines for development of future electron-injection based detectors as well as other heterojunction photodetectors. © *2016 AIP Publishing LLC*.
[http://dx.doi.org/10.1063/1.4944602]

Ultra-sensitive photon detectors in the short-wave infrared (SWIR) band have far-reaching consequences for a variety of diverse applications. This includes, but is not limited to quantum imaging, secure communication, medical imaging, homeland security, and non-destructive material evaluation.[1–3] To satisfy this growing need, significant amount of research has been devoted to the development of very sensitive SWIR detectors with ultra-low noise levels and high signal-to-noise ratios (SNRs). State-of-the-art semiconductor SWIR detectors include p-i-n detectors and avalanche photodetectors (APDs).

InGaAs p-i-n detectors have extremely low leakage current levels and short response times. Unfortunately, the lack of internal amplification in such detectors results in the overall system signal-to-noise ratio to be mostly limited by the preamplifier noise.[4] Avalanche photodetectors, on the other hand, are built based on an internal multiplication scheme, which is coupled to the detection mechanism.[5] InGaAs/InP APDs provide stable gain values of close to 3 at ∼25 V at room temperature.[6] Unfortunately, due to the internal positive feedback in the avalanche multiplication process, the gain tends to destabilize at higher values and increases amplitude uncertainty.[7]

Electron-injection based detectors address these shortcomings and operate in the linear-mode and at low bias voltages.[8] Figure 1(a) shows the schematic diagram of the detector. These detectors simultaneously provide high avalanche-free amplification, unity excess noise, and low leakage current.[9–12] Experimental results show that devices with 10 μm injector diameter and 30 μm absorber diameter provide a peak optical gain of ∼1000, dark current of ∼15 nA, and a fast rise time of ∼10 ns at ∼20 μW of optical power at a bias voltage of ∼−3 V and at room temperature.[13]

There are many design options possible for the electron-injection based detectors, both geometrically and in terms of different semiconductor layers composition and doping levels. Therefore, robust analytical models are very valuable as they present the relation of these parameters to important performance metrics such as response time, optical gain, and dark current. In this paper, we present our comprehensive analytical models for the detector speed and dark current. Furthermore, we have modified the optical gain model in Ref. 20 to take into account the high-injection effects. We have further modeled the detector numerically. The simulation software package used for this work is a commercial device simulator (ATLAS from Silvaco International). Good agreement between the published experimental data of a detector with 10 μm injector diameter, the analytical modeling, and the numerical simulations is observed. This agreement ensures good confidence in the reported material parameters. Also, the effect of scaling the injector diameter with respect to the absorber has been investigated.

The equilibrium energy band diagram as a function of depth along the central axis of the device is shown in Figure 1(b). Due to the doping gradients in the device, an internal electric field exists in the large InGaAs absorber, which becomes stronger when the device is appropriately biased. Upon absorption of a photon, an electron-hole pair is generated in the absorber. The electron and the hole are immediately separated by the internal electric field in the device,

[a)]Y. Movassaghi and V. Fathipour contributed equally to this work.

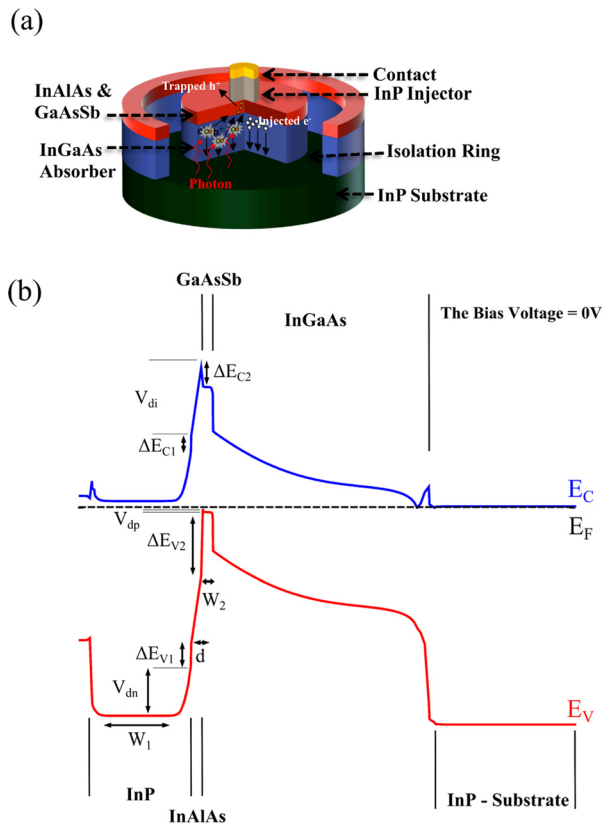

FIG. 1. (a) Schematic diagram of the electron-injection detector (b). The equilibrium energy band diagram of an isolated electron injection detector along a cutline through the central axis of the device.

and the hole then gets trapped in the GaAsSb trapping layer.[9] This leads to a change in the barrier potential, causing the injection of electrons towards the absorption layer, and hence, an internal gain is obtained. The holes that are trapped in the GaAsSb trapping layer will eventually recombine, relaxing the bands.

The numerical simulation model is based on the core drift-diffusion equations in three dimensions. The model involves solution of the five coupled general semiconductor equations using Newton-Raphson algorithm's technique. Boundary conditions were imposed by utilizing ohmic contacts. Furthermore, along the outer (non-contact) edges of devices, homogeneous (reflecting) Neumann boundary conditions were considered. Fermi-Dirac statistics were taken into account. Semiconductor was considered non-degenerate with uniform doping profiles. The model incorporates several nonlinear effects such as incomplete ionization of electrons and holes, surface recombination, concentration dependent mobility, band gap narrowing, and hot electron effects. Recombination mechanisms were approximated by concentration dependent Shockley-Read-Hall (SRH), as well as the radiative (the optical band-to-band) and Auger recombination models. Dense mesh is used where the gradients of the carrier concentration and electric fields are high. Material parameters employed in our numerical simulation model are based on published experimental parameters.[14–17] Table I shows the parameter values used in the numerical simulation.[18] To obtain a good qualitative agreement between the results obtained from numerical simulation and those obtained from the experimental measurement, a band gap smaller than what is typically reported for the InAlAs layer was utilized.[14] This can be attributed to the unwanted change of alloying mole fraction of InAlAs by Sb ions in the chamber during the deposition period of this layer. Furthermore, simulation results predict that incorporation of radiative generation/recombination does not affect our results appreciably. Radiative recombination rate in our structure is intrinsic to the bulk material, while other recombination channels (namely, surface and SRH recombination lifetimes) are heavily material quality and processing dependent. At the current stage, with the material properties and the device geometry we have, SRH channel appears to be much faster, and thus, the effect of radiative recombination is negligible. Improved device performance is thus expected once improvement in material quality/fabrication process is obtained. The surface recombination velocities for electrons (S_n) and holes (S_p) at the interfaces were assumed as 10^4 cm/s and 10^2 cm/s, respectively, in our numerical modeling.

As shown in Figure 1(b), in the electron-injection detector, the conduction band-edge discontinuity ($\Delta E_C = \Delta E_{C1} + \Delta E_{C2}$), the valence band-edge discontinuity ($\Delta E_V = \Delta E_{V1} + \Delta E_{V2}$), and the total built-in potential ($V_d = V_{dn} + V_{di} + V_{dp}$) are related.[18,19] V_{dn}, V_{dp}, and V_{di} are the barriers corresponding to band bending on the n^+, p^+, and on the undoped InAlAs sides. The detector dark current has two major components, diffusion (I_{DIFF}) and generation-recombination (I_{GR}).

TABLE I. Parameters used in the numerical device simulation model.[14]

Parameter	Symbol	InP	$In_{0.53}Ga_{0.47}As$	$In_{0.52}Al_{0.48}As$	$GaAs_{0.52}Sb_{048}$
Energy gap (eV)	Eg	1.35	0.754	1.3107	0.787
Electron affinity (eV)	χ	4.35	4.58	4.25	4.35
Permittivity	$\varepsilon_r/\varepsilon_0$	12.4	13.5	12.3	14.3
Electron effective density of states (cm^{-3})	N_C	5.4×10^{17}	2.1×10^{17}	5.2×10^{17}	2.4×10^{17}
Hole effective density of state (cm^{-3})	N_V	1.3×10^{19}	8.9×10^{18}	1.2×10^{19}	7.5×10^{18}
Electron effective mass	m_n^*/m_0	0.077	0.041	0.075	0.045
Hole effective mass	m_p^*/m_0	0.5	0.47	0.47	0.456
Electron mobility ($cm^2/V\,s$)	μ_n	5700	18200	5100	5850
Hole mobility ($cm^2/V\,s$)	μ_p	210	370	190	80
Minority carrier life time (ns)	τ_n or τ_p	1	10	0.01	1
Doping concentration (cm^{-3})	N_A *or* N_D	10^{17}	1×10^{15}	2×10^{16}	5×10^{18}
Layer thickness (nm)	d	500	1000	50	50

The diffusion components of current density for electrons and holes in the neutral regions can be expressed as[18,19]

$$I_{sn} = \frac{qAn_{ip}^2}{N_A}\sqrt{\frac{\mu_n k_B T}{q\tau_n}}\frac{\frac{S_n L_n}{D_n}\cosh\left(\frac{W_2}{L_n}\right)+\sinh\left(\frac{W_2}{L_n}\right)}{\frac{S_n L_n}{D_n}\sinh\left(\frac{W_2}{L_n}\right)+\cosh\left(\frac{W_2}{L_n}\right)} \times \exp\left(\frac{-q(V_d+\Delta E_C)}{k_B T}\right), \quad (1)$$

$$I_{sp} = \frac{qAn_{in}^2}{N_D}\sqrt{\frac{\mu_p k_B T}{q\tau_p}}\frac{\frac{S_p L_p}{D_p}\cosh\left(\frac{W_1}{L_p}\right)+\sinh\left(\frac{W_1}{L_p}\right)}{\frac{S_p L_p}{D_p}\sinh\left(\frac{W_1}{L_p}\right)+\cosh\left(\frac{W_1}{L_p}\right)} \times \exp\left(\frac{-q(V_d+\Delta E_V)}{k_B T}\right), \quad (2)$$

where n_{in}, n_{ip} are the intrinsic carrier concentrations in the n^+ InP and p^+ GaAsSb regions, and N_A, N_D are the acceptor and donor concentrations, respectively, in the p^+ GaAsSb and n^+ InP regions. A is the injector area, q is the electron charge, k_B is the Boltzmann constant, T is the temperature, μ_p and μ_n are the hole and electron mobilities, respectively. τ_p and τ_n are the hole and electron life times, and L_p and L_n are the diffusion lengths of holes and electrons on n^+ and p^+ sides, respectively. W is the quasi natural region width, W_1 is the width of undepleted InP injector layer, and W_2 is the width of undepleted GaAsSb trap layer. The total diffusion current can be expressed as[18]

$$I_{DIFF} = (I_{sn} + I_{sp})\left(\exp\left(\frac{qV}{k_B T}\right) - 1\right). \quad (3)$$

The generation-recombination component of current in the depletion region can be expressed as[18,19]

$$I_{GR} = 2\sqrt{3(k_B T)^3}\sigma N_f\left[\frac{n_{in}x_n}{V_{dn}}\sqrt{\frac{1}{m_{nn}^*}} + \frac{n_{ip}x_p}{V_{dp}}\sqrt{\frac{1}{m_{pp}^*}} + \frac{n_i d}{V_{di}}\sqrt{\frac{1}{m_{n0}^*}}\right]\exp\left(\frac{qV}{2k_B T}\right), \quad (4)$$

where x_n and x_p are the widths of depletion regions in InP and GaAsSb and d is the InAlAs thickness. n_i is the intrinsic carrier concentration in InAlAs region. m_{nn}^*, m_{n0}^*, and m_{pp}^* are the effective masses of electrons and holes in the InP and InAlAs and GaAsSb regions, respectively. Details of the derivation of the dark current model and the parameters used in the analytical modeling are provided in Ref. 18.

Figure 2(a) shows the dark current ($I_{DARK} = I_{DIFF} + I_{GR}$) characteristic of an electron-injection based detector with 10 μm injector at different temperatures. The experimental data is obtained from the data reported in Ref. 13. There is qualitative agreement between dark current obtained from the analytical model, simulation, and experimental measurement at all temperatures. The dark current after amplification is ~15 nA at room temperature, decreasing to ~500 fA at 160 K.

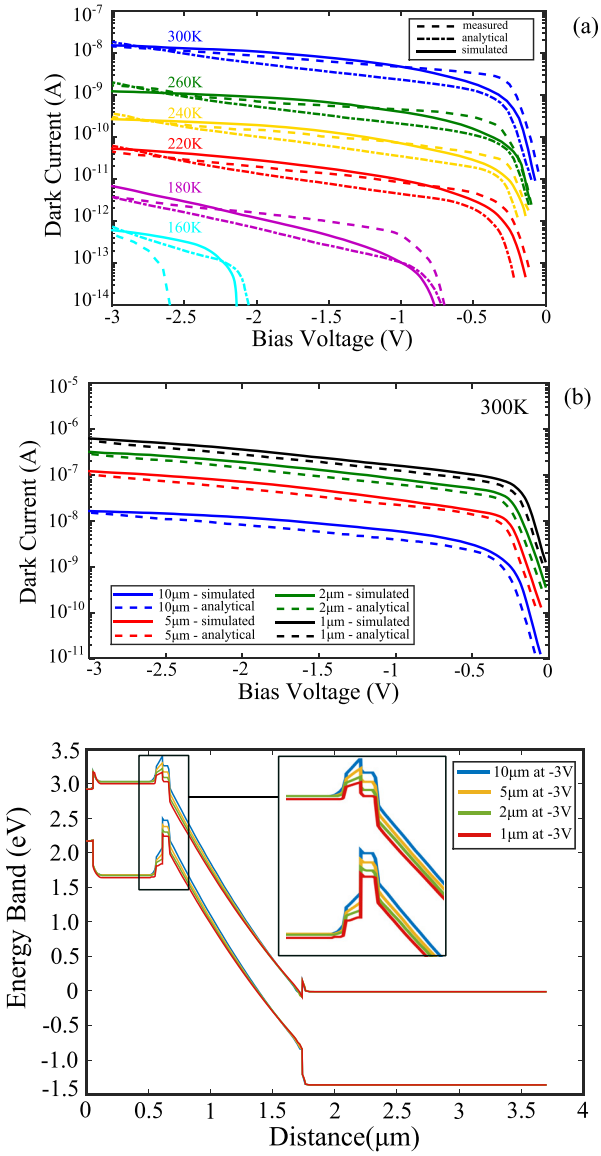

FIG. 2. (a) Dark current versus bias voltage characteristics of the electron-injection detector with 10 μm injector and 30 μm absorber diameter at different temperatures. Good agreement exists between analytical modeling, simulation, and experimental measurement data of Ref. 13. (b) The dark current versus bias voltage characteristics for different injector diameters. A device with 1 μm injector diameter exhibits dark current of ~500 nA at −3 V. (c) The energy band diagram of an isolated electron injection detector along a cutline through the central axis of the device for different injector diameters (Bias Voltage = −3 V).

Figure 2(b) shows the effect of scaling the injector diameter on the detector dark current. We assume that the bulk and surface parameters will be the same for smaller injectors as the 10 μm injector parameters. Both the analytical model and the numerical simulation results suggest that a device with 1 μm injector diameter exhibits dark current of ~500 nA at −3 V. Simulation results indicate that, as the injector diameter is reduced, the hole concentration in InAlAs layer increases. Increasing hole concentration causes the barrier potential to drop more pronouncedly in the conduction band and as such, the dark current increases with reduction in injector diameter (Fig. 2(c)).

For the optical gain ($G_{opt}(P)$) of the detector, we have utilized the analytical model introduced in Ref. 20. However, we have taken into account the reduction in the gain at high power levels by incorporating in the model

high-level injection effect in the GaAsSb layer, through an ideality factor that depends on the power (P) using $\eta_F(P)$[18]

$$G_{opt}(P) = \frac{G_{Max}\left[e^{\frac{qV_{BE}(P)}{\eta_F(P)k_BT}} - 1\right]}{\left[e^{\frac{qV_{BE}(P)}{\eta_F(P)k_BT}} - 1\right] + G_{Max}\frac{J_{SE}}{J_S}\frac{A}{A_B}\left[e^{\frac{qV_{BE}(P)}{\eta_E k_BT}} - 1\right]}. \quad (5)$$

In (5), J_{SE}/J_S demonstrates the ratio of saturation current density for recombination in the injector/trapping layer space charge region to saturation current density injected to the absorber, A/A_B demonstrates the ratio of injector to absorber area, and G_{Max} is the maximum optical gain. To calculate the responsivity of the detector, a continuous-wave monochromatic collimated source at 1550 nm wavelength was defined in our numerical simulator. The beam was applied at normal incidence angle to the device surface. Detector responsivity was obtained from the simulated dark and photocurrent data.

Figure 3(a) shows qualitative agreement between the optical gain versus power characteristic, obtained through numerical simulations and analytical modeling. For comparison purposes, the reported experimental data in Ref. 20 for an electron-injection detector with 10 μm injector is also provided. The drop of the optical gain at a low-light-level condition is due to the dominant recombination mechanisms in the space charge region

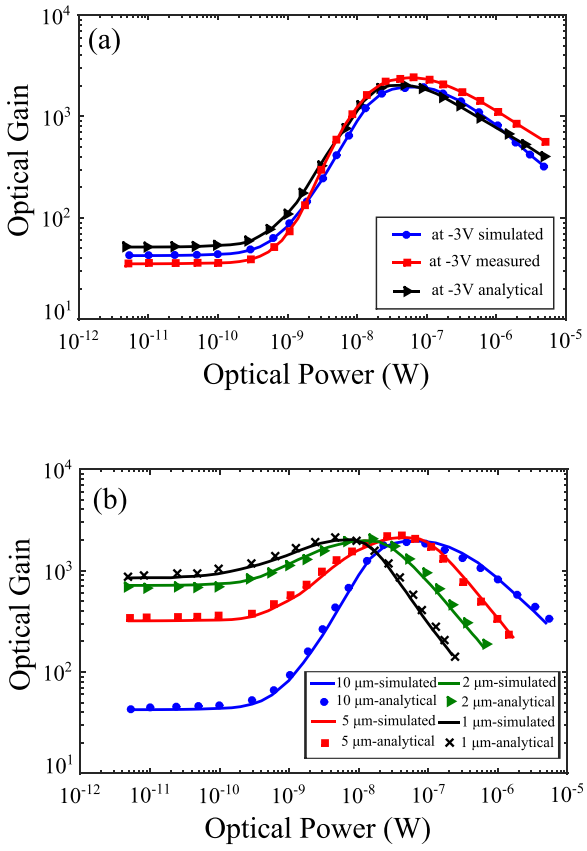

FIG. 3. (a) Optical gain versus optical power characteristic for an electron-injection based detector with 10 μm injector and 30 μm absorber diameter: Good agreement exists between results obtained by our numerical simulation, analytical modeling, and measurement.[20] Reproduced with permission from V. Fathipour, S. J. Jang, I. H. Nia, and H. Mohseni, "Impact of 3D Geometry on Performance of Electron-injection Infrared Detectors," Appl. Phys. Lett. **106**, 021116 (2015). Copyright 2015 AIP Publishing LLC. (b) Scaling the injector diameter with respect to the absorber diameter results in the drop in the optical gain to be shifted to lower optical power levels. Furthermore, a smaller injector device achieves a higher low-light-level-gain value.

of the injector/trapping layer heterojunction.[20] Figure 3(b) shows that the drop in the gain shifts to a lower power level for a smaller injector device. This is the result of a reduced recombination current in the injector/trap depletion region of a scaled injector device.[20] Similar behavior has also been observed in heterojunction-bipolar-phototransistors.[21] This figure also demonstrates that for a reduced injector size, a larger value of optical gain would be obtained at lower light intensities.

Rise time, (τ_{rise}), is defined as the time required for the detector signal to increase from the 10% to 90% of its final value, in response to a rectangular input light pulse. Rise time of the electron-injection detector has been modeled using (6)[18,22]

$$\tau_{rise} = 2.2\left(\tau_e + G_{opt}R_TC_{pn} + \frac{G_{opt}\tau_{ce}}{2}\right) + \left(2.2 + \ln\left\{\frac{I_{dark} + 0.9i_{ph}}{I_{dark} + 0.1i_{ph}}\right\}\right)\frac{k_BT}{q(I_{dark} + i_{ph})}C_T, \quad (6)$$

where I_{dark} and i_{ph} are the internal dark and photocurrents, R_T is the total emitter resistance, τ_e is the minority-electron lifetime in the GaAsSb layer, τ_b is the GaAsSb transit time $\tau_e = G_{opt} \times \tau_b$, and τ_{ce} is transient time in the absorber layer. C_T is the sum of the junction capacitance in the InP/InAlAs/GaAsSb (C_{pin}) and the junction capacitance in the GaAsSb/InGaAs (C_{pn}) layers, i.e., $C_T = C_{pin} + C_{pn}$. In this model, C_{pn} and C_T are taken as fitting parameters. To obtain the rise time of the detector, from the implemented structure in the numerical simulator, a pulsed monochromatic collimated source at 1550 nm wavelength was used. Fig. 4 depicts the rise time versus optical power plot as obtained on the basis of the model (shown by dashed lines) and that from the simulation results (shown by solid lines). The parameters used in the analytical modeling are discussed in detail in Ref. 18.

Upon increasing optical power, internal photocurrent (i_{ph}) increases and as a result, rise time decreases. At optical power of ~10 μW, a rise time of ~30 ns is achieved for a detector with 10 μm diameter injector. Reducing the injector size reduces the injector junction capacitance (C_{pin}) and as a result C_T is reduced. For a detector with 1 μm injector diameter at optical power of ~10 μW, rise time of ~400 ps is predicted.

Finally, results of sensitivity analysis for this device are presented in Table II. This analysis is helpful for local optimization of device parameters. For each variable, X, the sensitivity S_X to changes in parameter p is defined as $(\Delta X/\Delta p)(p/X)$, where ΔX

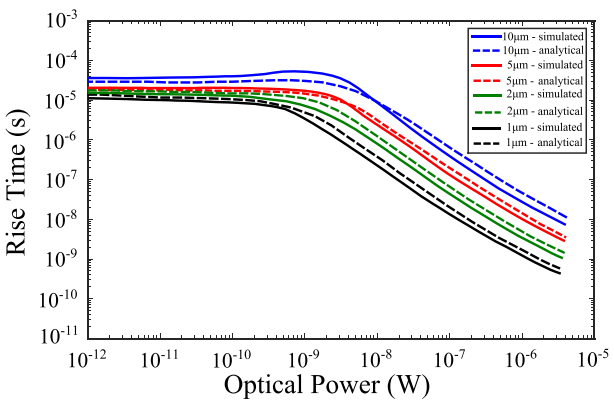

FIG. 4. Numerical simulation and analytical modeling of rise time versus optical power for electron injection detectors with different injector diameters.

TABLE II. Sensitivity analysis.

	InGaAs			InAlAs			GaAsSb		
Parameter	S_{Gopt} (at $P = 10^{-11}$ W)	$S_{\tau rise}$	S_{Idark}	S_{Gopt} (at $P = 10^{-11}$ W)	$S_{\tau rise}$	S_{Idark}	S_{Gopt} (at $P = 10^{-11}$ W)	$S_{\tau rise}$	S_{Idark}
τ_n *or* τ_p	−1.76	0.0952	−2.37	2.67	0.0357	2.23	0.0665	0.0119	0.0291
N_A *or* N_D							−4.37	0.00595	−2.17
d				−3.989	0.0595	−3.12	0.664	0.0297	0.447
Semiconductor/air boundary									
Sn	0.0042	0.00062	0.00683						
Sp	0.0182	0.00075	0.0235						

represents small variation in variable X obtained as a result of variation in the parameter p by Δp. For example, to improve the gain, acceptor concentration in GaAsSb layer should be decreased. This would, however, increase the dark current. A decrease in the InAlAs layer thickness would also improve the optical gain, while it would increase the dark current.

In summary, we developed comprehensive analytical models for the detector response time, dark current, and gain. These models provide insight into the relative importance of the detector parameters and the interplay between them to optimize the detector design and to explain various physical mechanisms that shape detector characteristics. We have also numerically modeled the detector with a commercial simulation tool. The results from analytical models and numerical simulation are compared with the published experimental data. Good agreement between analytical modeling, simulation, and measurement data is obtained, suggesting good confidence in the reported material parameters. Furthermore, enhancements in device performance such as gain and speed are anticipated by reducing the injector diameter. The sensitivity analysis identifies important parameters for optimization of device, as well as the direction that the parameter should be changed (this analysis holds for local optimization rather than a global optimization). For example, to improve the gain, acceptor concentration in GaAsSb layer should be decreased. This would, however, increase the dark current. A decrease in the InAlAs layer thickness would also improve the optical gain, while it would increase the dark current.

V.F. and H.M. would like to acknowledge the partial support from NSF Award No. ECCS-1310620, as well as the computational resources and staff contributions provided for the Quest high performance computing facility at Northwestern University, which is jointly supported by the Office of the Provost, the Office for Research, and Northwestern University Information Technology. V.F. would also like to acknowledge the Ryan Fellowship support from Northwestern University. Y.M. and M.F. would like to acknowledge partially support by Nanoelectronic Center of Excellence at department of electrical and computer engineering at University of Tehran.

[1]R. M. Marino, W. R. Davis, G. C. Rich, J. L. Mclauling, E. L. Lee, B. M. Stanley, J. W. Burnside, G. S. Rowe, R. E. Hatch, T. E. Square, L. J. Skelly, M. O'Brien, A. Vasile, and R. M. Heinrichs, "High-resolution 3D imaging laser radar flight test experiments," Proc. SPIE **5791**, 138–151 (2005).
[2]E. Knill, R. Laflamme, and G. J. Milburn, "A scheme for efficient quantum computation with linear optics," Nature **409**, 46–52 (2001).
[3]E. Diamanti, C. Langrock, M. M. Fejer, Y. Yamamoto, and H. Takesue, "1.5 μm photon-counting optical time-domain reflectometry with a single photon detector based on upconversion in a periodically poled lithium niobate waveguide," Opt. Lett. **31**, 727–729 (2006).
[4]A. Poloczek, M. Weiss, S. Fedderwitz, A. Stoehr, W. Prost, D. Jaeger, and F. J. Tegude, "Integrated InGaAs pin-diode on exactly oriented silicon (001) substrate suitable for 10 Gbit/s digital applications," in *Proceedings of the 20th Annual Meeting of the IEEE LEOS* (2007), pp. 180–181.
[5]S. Cova, M. Ghioni, A. Lotito, I. Rech, and F. Zappa, "Evolution and prospects for single-photon avalanche diodes and quenching circuits," J. Mod. Opt. **51**(9/10), 1267–1288 (2004).
[6]N. Duan, S. Wang, X. G. Zheng, X. Li, N. Li, J. C. Campbell, C. Wang, and L. A. Coldren, "Detrimental effect of impact ionization in the absorption region on the frequency response and excess noise performance of InGaAs-InAlAs SACM avalanche photodiodes," IEEE J. Quantum Electron. **41**(4), 568–572 (2005).
[7]R. J. McIntyre, "Multiplication noise in uniform avalanche diodes," IEEE Trans. Electron Devices **13**, 164–168 (1966).
[8]O. G. Memis, A. Katsnelson, S. C. Kong, H. Mohseni, M. Yan, S. Zhang, T. Hossain, N. Jin, and I. Adesida, Appl. Phys. Lett. **91**, 171112 (2007).
[9]V. Fathipour, O. G. Memis, S. J. Jang, F. Khalid, R. Brown, I. H. Nia, R. M. Gelfand, and H. Mohseni, "Isolated nanoinjection photo detectors for high-speed and high-sensitivity single-photon detection," Proc. SPIE **8868**, 886803 (2013).
[10]V. Fathipour, S. J. Jang, I. H. Nia, and H. Mohseni, "Approaching high temperature photon counting with electron-injection detectors," SPIE Proc. **9220**, 92200J (2014).
[11]O. G. Memis, A. Katsnelson, S. C. Kong, H. Mohseni, M. Yan, S. Zhang, T. Hossain, N. Jin, and I. Adesida, "Sub-poissonian shot noise of a high internal gain injection photon detector," Opt. Express **16**(17), 12701 (2008).
[12]V. Fathipour, S. J. Jang, R. Brown, and H. Mohseni, "Highly sensitive and linear electron-injection detectors at the telecom wavelength," in *Frontier in Optics* (Optical Society of America, 2014), p. FW2A.4, https://www.osapublishing.org/abstract.cfm?uri=fio-2014-FW2A.4.
[13]V. Fathipour, O. G. Memis, S. J. Jang, R. L. Brown, I. H. Nia, and H. Mohseni, "Isolated electron injection detectors with high gain and record low dark current at telecom wavelength," IEEE J. Sel. Top. Quantum Electron. **20**(6), 1–6 (2014).
[14]I. Vurgaftman and J. R. Meyer, "Band parameters for IIIV compound semiconductors and their alloys," Appl. Phys. Rev. **89**(11), 5815 (2001).
[15]J. Bohrer, M. Grundmann, U. Lienert, D. Bimberg, H. Ishikawa, M. Kamada, and N. Watanabe, "Determination of the band discontinuity of MOCVD grown $In_{1-x}Ga_xAs/In_{1-y}Al_yAs$ heterostructures with optical and structural methods," J. Cryst. Growth **107**, 555–560 (1991).
[16]M. J. Martinez, D. C. Look, J. R. Sizelove, and F. L. Schuermeyer, "Monte Carlo simulation of bulk hole transport in $Al_xGa_{1-x}As$, $In_{1-x}Al_{1-x}As$ and $GaAs_xSb_{1-x}$," J. Appl. Phys. **77**, 661–664 (1995).
[17]S. Datta, S. Shi, K. P. Roenker, M. M. Cahay, and W. E. Stanchina, "Simulation and design of InAlAs/InGaAs pnp heterojunction bipolar transistors," IEEE Trans. Electron Devices **45**, 1634–1643 (1998).
[18]Y. Movassaghi, V. Fathipour, M. Fathipour, and H. Mohseni, "Analysis, modeling and simulation of electron-injection detectors," J. Appl. Phys. (unpublished).
[19]P. Chakrabarti, A. Krier, and A. F. Morgan, "Analysis and simulation of a mid-infrared P^+-$InAs_{0.55}Sb_{0.15}P_{0.30}$/n0-$InAs_{0.89}Sb_{0.11}$/$N^+$-$InAs_{0.55}Sb_{0.15}P_{0.30}$ double heterojunction photodetector grown by LPE," IEEE Trans. Electron Devices **50**, 2049–2058 (2003).
[20]V. Fathipour, S. J. Jang, I. H. Nia, and H. Mohseni, Appl. Phys. Lett. **106**, 021116 (2015).
[21]M. S. Park and J. H. Jang, IEEE Photonics Technol. Lett. **22**, 1202–1204 (2010).
[22]J. P. Helme and P. A. Houston, "Analytical modeling of speed response of heterojunction bipolar phototransistors," J. Lightwave Technol. **25**(5), 1247–1255 (2007).